Tyrosine Kinase Inhibition Alters Intratumoral CD8$^+$ T-cell Subtype Composition and Activity

Andrew D. Tieniber, Andrew N. Hanna, Benjamin D. Medina, Gerardo A. Vitiello, Mark S. Etherington, Mengyuan Liu, Kevin J. Do, Ferdinando Rossi, and Ronald P. DeMatteo

ABSTRACT

Targeted therapy with a tyrosine kinase inhibitor (TKI) such as imatinib is effective in treating gastrointestinal stromal tumor (GIST), but it is rarely curative. Despite the presence of a robust immune CD8$^+$ T-cell infiltrate, combining a TKI with immune-checkpoint blockade (ICB) in advanced GIST has achieved only modest effects. To identify limitations imposed by imatinib on the antitumor immune response, we performed bulk RNA sequencing (RNA-seq), single-cell RNA-seq, and flow cytometry to phenotype CD8$^+$ T-cell subsets in a genetically engineered mouse model of GIST. Imatinib reduced the frequency of effector CD8$^+$ T cells and increased the frequency of naïve CD8$^+$ T cells within mouse GIST, which coincided with altered tumor chemokine production, CD8$^+$ T-cell recruitment, and reduced CD8$^+$ T-cell intracellular PI3K signaling. Imatinib also failed to induce intratumoral T-cell receptor (TCR) clonal expansion. Consistent with these findings, human GISTs sensitive to imatinib harbored fewer effector CD8$^+$ T cells but more naïve CD8$^+$ T cells. Combining an IL15 superagonist (IL15SA) with imatinib restored intratumoral effector CD8$^+$ T-cell function and CD8$^+$ T-cell intracellular PI3K signaling, resulting in greater tumor destruction. Combination therapy with IL15SA and ICB resulted in the greatest tumor killing and maintained an effector CD8$^+$ T-cell population in the presence of imatinib. Our findings highlight the impact of oncogene inhibition on intratumoral CD8$^+$ T cells and support the use of agonistic T-cell therapy during TKI and/or ICB administration.

Introduction

Gastrointestinal stromal tumor (GIST) is the most common human sarcoma with an annual U.S. incidence of about 6,000 (1, 2). GIST is usually driven by a single mutation in the *KIT* or *PDGFRA* tyrosine kinase receptor genes. The introduction into the clinic of imatinib, a tyrosine kinase inhibitor (TKI) of the Kit and Pdgfra oncoproteins, has increased the median survival of patients with advanced GIST from 1 year to over 5 years (3–5). Unfortunately, imatinib is rarely curative, and tumor progression occurs at a median of 18 months, typically due to secondary *KIT* mutations (6–8). Second- and third-line TKIs such as sunitinib and regorafenib are effective, but the median time to tumor progression is only 5 to 7 months (9, 10). Conventional cytotoxic chemotherapy is not effective in GIST (11). Therefore, new approaches are needed for this cancer.

We (12–17) and others (18, 19) have reported on the robust immune infiltrate in GIST. CD8$^+$ T cells in GIST restrain tumor growth and have high PD1 expression (12, 15). Furthermore, imatinib potentiates the antitumor T-cell response in part through the inhibition of indoleamine 2,3-dioxygenase (IDO) production (12). Immunotherapies have been tested in clinical trials involving patients with advanced GIST resistant to more than two TKIs. Ipilimumab (anti–CTLA-4) plus dasatinib (TKI) resulted in limited clinical efficacy, although tumor IDO suppression may have correlated with an antitumor response (20). More recently, nivolumab (anti–PD-1) was tested alone and in combination with ipilimumab, but without a TKI. Although the median progression-free survival (PFS) of patients in the nivolumab and nivolumab + ipilimumab arm was limited at 11.7 and 8.3 weeks, respectively, there was a subset of patients with a PFS of >2 years (n = 3/36; ref. 21). Thus, immunotherapy has not been effective so far in GIST patients, at least using conventional T-cell checkpoint inhibitors.

Given the efficacy of imatinib in GIST, T-cell immunotherapy would ideally be used in combination with a TKI. However, the interplay between Kit or Pdgfra inhibition and the immune response is complex. First, mutation type (*KIT* or *PDGFRA*) influences overall intratumoral immunogenicity, with Pdgfra-mutant GISTs harboring more immune cells with greater cytolytic activity compared with Kit-mutant GISTs (16, 18). Pdgfra- and Kit-mutant GISTs also express distinctive cytokine profiles with different driver-derived neoepitopes, which may affect an immune-checkpoint blockade (ICB) approach (16). Second, imatinib therapy in mouse and human GIST reduces the frequency of tumor-associated macrophages (TAM) and skews them to an M2 phenotype (13). Finally, imatinib restricts the frequency of intratumoral Batf3$^+$ (CD141$^+$ in humans) dendritic cells (DC), which limits the antitumor effect of CD8$^+$ T cells (13, 14).

In this study, we sought to further examine CD8$^+$ T cells in GIST to better understand and combat the limitation of T-cell immunotherapy in the presence of a TKI. Through traditional and next-generation sequencing methods, we found that intratumoral CD8$^+$ T cells have a clear effector memory profile at baseline that is altered to a naïve subtype following imatinib treatment. Additionally, imatinib therapy reduced intratumoral CD8$^+$ T-cell intracellular PI3K signaling and failed to induce T-cell clonal expansion, likely due to its effects on antigen-presenting cells. An IL15 superagonist (IL15SA) supported the antitumor and memory profile of CD8$^+$ T cells in the presence of imatinib, and combination therapy with IL15SA and ICB resulted in the greatest tumor killing and maintained an effector CD8$^+$ T-cell population in the presence of imatinib. Last, we found a similar effect of imatinib therapy on CD8$^+$ T-cell subsets in human GIST surgical specimens. Overall, our results indicate the need for T-cell agonism in the immunotherapy of GIST treated with a targeted molecular agent.

Perelman School of Medicine, Department of Surgery, University of Pennsylvania, Philadelphia, Pennsylvania.

Corresponding Author: Ronald P. DeMatteo, Perelman School of Medicine, University of Pennsylvania, Philadelphia, PA 19104. Phone: 215-662-7539; Fax: 215-614-0363; E-mail: dematter@.upenn.edu

Cancer Immunol Res 2022;10:1210–23

doi: 10.1158/2326-6066.CIR-21-1039

Materials and Methods

Mice

Eight- to 12-week-old *Kit*$^{V558\Delta/+}$ mice (22) on a C57BL/6 background, C56BL/6 mice, as well as congenic CD45.1 mice (Jackson Laboratory), were maintained in a pathogen-free animal facility, and age- and sex-matched for experiments to ensure similar tumor sizes. The animal experiments were approved by the Institutional Animal Care and Use Committee at the University of Pennsylvania.

Treatments

Imatinib mesylate (Novartis) was dissolved in the drinking water at 600 mg/L and provided ad lib as previously described (14). For *in vivo* IL15 stimulation, 1.5 μg IL15 (210-15, PeproTech) was incubated with 7 μg IL15Ra (551-MR, R&D Systems) for 30 minutes at 37°C as previously described (23). IL15:IL15Ra (referred to as IL15SA) or PBS was administered i.p. on days −2, 2, and 6 relative to the initiation of treatment with vehicle/imatinib. For *in vivo* CD8 depletion during IL15SA or imatinib therapy, 200 μg of anti-mouse CD8α (BE0061, Bio X Cell) or anti-rat IgG2b (BE0090, Bio X Cell) was administered i.p. on days −5, −4, −3, 1, and 5 relative to initiation of treatment with vehicle/imatinib. For concurrent IL15SA and anti–PD-1 (aPD1) therapy, Il15SA, 250 μg aPD1 (RMP1–14, Bio X Cell), PBS, or anti-rat IgG2a (2A3, Bio X Cell) was administered i.p. on days −2, 2, and 6 relative to initiation of treatment with vehicle/imatinib and every 4 days until day 28.

For adoptive transfer experiments, 200 μg of anti-mouse CD8α (BE0061, Bio X Cell) was administered to *Kit*$^{V558\Delta/+}$mice i.p. on day 0, followed by 600 mg/L imatinib or vehicle for 5 days. On day 4, splenic CD8$^+$ T cells were isolated from CD45.1 mice by bead sorting (Miltenyi Biotec, cat. #130-104-075) and labeled with CFSE (Invitrogen, cat. #C34554) according to the manufacturer's instructions. 2×10^6 CD45.1 CD8$^+$ T cells were adoptively transferred to each *Kit*$^{V558\Delta/+}$ mouse via retroorbital injection. Mice were sacrificed 24 hours later on day 5, and the cell number was counted using counting beads (Invitrogen, cat. #C36950).

For *in vitro* experiments, splenic CD8$^+$ T cells were isolated from C57BL/6 mice by bead sorting (Miltenyi Biotec, cat. #130-104-075). Purity was > 90% by flow cytometry (see "Flow cytometry"). Using 96-well plates, 8×10^4 CD8$^+$ T cells were cultured in serum-complete RPMI medium [RPMI modified with glutamine, HEPES, and phenol red (Gibco, cat. #22400089), and supplemented with 10% FCS (Lab Force, cat. #FB5002-H), 0.05 mmol/L β-mercaptoethanol (Sigma-Aldrich, cat. #M3148), and 1× penicillin–streptomycin (Gibco, cat. #15140–122)] with CD3/CD28 microbeads (Dynabeads, cat. #11456D), as per the manufacturer's protocol. Cells were treated with vehicle (H_2O) or 50 nm imatinib for 6 hours prior to analysis.

Preparation of cell suspensions

Excised tumors, spleens, and lymph nodes were minced and incubated in Liberase TL (Roche, cat. #C790D66) and prepared into single-cell suspensions as previously described (14). There is one main mesenteric draining lymph node in *Kit*$^{V558\Delta/+}$ mice. Cells were analyzed by flow cytometry or prepared for bulk RNA sequencing (RNA-seq) or single-cell RNA-seq (scRNA-seq; see **Flow cytometry** and **Bulk RNA-seq, scRNA-seq, and bioinformatics**). For the isolation of CD8$^+$ T cells from *Kit*$^{V558\Delta/+}$ mice, CD45$^+$CD3$^+$NK1.1$^-$CD4$^-$CD8$^+$ cells were sorted directly into TRIzol LS Reagent (Life Technologies, cat. #10296028) using a FACSAria II flow cytometer (BD Biosciences).

Flow cytometry

Flow cytometry was performed with an LSRFortessa (BD) and analyzed using FlowJo v10 (BD). Fc receptor blockade was achieved with anti-CD16/32 (clone 2.4G2, Bio X Cell). Mouse-specific antibodies conjugated to various fluorochromes were purchased from BioLegend (CD45, clone 30-F11; Tbet, clone 4B10), BD Biosciences (CD44, clone IM7; CD117, clone 2B8; CD62L, clone MEL14; NK1.1, clone PK136; CD4, clone GK1.5; CD3, clone 145-2C11; and CD45.1, clone A20), eBioscience (CD8, clone 53-6.7; CD40, clone 1C10; Ki67, clone SolA15; PD1, clone J43; and CD103, clone 2E7), and Invitrogen (granzyme B, clone NGZB; propidium iodide, cat. #556463; phospho-AKT1, clone SDRNR; phosphor-mTOR, clone MRRBY). Human-specific antibodies conjugated to various fluorochromes were purchased from BioLegend (CD45, clone HI30; CD45RO, clone UCHL1), BD Biosciences (PD1, clone MIH4; CD45RA, clone HI100; CD3, clone SK7; CD56, clone B159; CD19, clone HIB19; CD4, clone RPA-T4; and CD8, clone RPA-T8). Intracellular cytokine staining was performed with the Cytofix/Cytoperm Kit (BD Biosciences). CFSE staining was performed using the Invitrogen CFSE Cell Proliferation Kit (cat. #C34554), as directed. Annexin V staining was performed using the eBioscience Annexin V staining kit (cat. #88-8103-72), as directed. CD8$^+$ effector memory T cells (T_{EM}) were defined as CD45$^+$CD3$^+$NK1.1$^-$CD4$^-$CD8$^+$CD44$^+$CD62L$^-$, central memory (T_{CM}) as CD45$^+$CD3$^+$NK1.1$^-$CD4$^-$CD8$^+$CD44$^+$CD62L$^+$, naïve (T_N) as CD45$^+$CD3$^+$NK1.1$^-$CD4$^-$CD8$^+$CD44$^-$CD62L$^+$, and resident as CD103$^+$ (24).

Microscopy

Tissues were formalin-fixed and embedded in paraffin. 5-μm tissue sections were mounted on glass slides by the Veterinary Medicine Comparative Pathology Core. Routine hematoxylin and eosin staining was performed. Slides were scanned with an Aperio VERSA 200 platform at the University of Pennsylvania School of Veterinary Medicine Comparative Pathology Core.

TCRβ sequencing

DNA extraction of fresh frozen tumor, spleen, and cecum tissue from *Kit*$^{V558\Delta/+}$ mice treated with either vehicle or imatinib was performed using the DNeasy Blood and Tissue Kit (Qiagen, cat. #69504) according to the manufacturer's instructions. Samples were analyzed by Adaptive Biotechnologies by high-throughput sequencing of the CDR3 TCRβ region using the ImmunoSEQ assay (Adaptive Biotechnologies). Immunologic endpoints including unique productive sequences and clonality were assessed through previously described methods (25).

Bulk RNA-seq, scRNA-seq, and bioinformatics

Next-generation RNA-seq of approximately 20,000 sorted CD8$^+$ T cells from spleen, tumor-draining lymph node, or tumor from *Kit*$^{V558\Delta/+}$ mice treated with vehicle or imatinib was performed by the institutional Integrated Genomics Operations core facility using an Illumina HiSeq 2,500 platform (4/group). Tissue was first processed into single-cell suspensions (see **Preparation of cell suspensions**), and sorted cells were provided to the Integrated Genomics Operations core for analysis. We obtained a minimum of 40 to 50 million reads per sample, with a read length of 50 bp with paired ends. Sequencing reads were then aligned to the mouse genome (mus musculus, GRCm38.p6), and gene-level counts were calculated using STAR version 2.6.1b. Raw counts were then normalized, and differential gene expression was performed using the R software package DESeq2. GSEA was performed using the java GSEA software package (version 3.0) and Molecular Signatures Database (Broad Institute).

We processed six tumors from 10-week-old $Kit^{V558\Delta/+}$ mice into single-cell suspensions (see "Preparation of cell suspensions"). Mice had been treated with vehicle or imatinib for one week (3/group). FACS on a FACSAria Fusion (BD) was used to collect live 7-AAD$^-$CD45$^+$ cells. Then, purified cell suspensions were submitted to the Center for Applied Genomics at the Children's Hospital of Philadelphia for scRNA-seq on the 10x Genomics platform.

The scRNA-seq reads were aligned to the GRCm38/mm10 reference genome and processed using Cellranger (10x Genomics, version 3.1). Downstream analyses were performed with the R package Seurat version 3.0 (26). Cells with fewer than 200 genes, more than 2,500 genes, or more than 10% mitochondrial RNA content were excluded from further analysis, resulting in 50,263 of 55,085 cells used for downstream analysis (91.2%).

To cluster all the cell types within the data set, the package sctransform (27) was used to perform normalization, variance stabilization, and variable feature selection on each sample separately. The function "IntegrateData" was used to combine all cells from the 6 samples into one data set for downstream clustering and comparison while eliminating batch effects and technical variation, where anchors identified and conserved across all 6 samples are used to map all the cells onto one harmonized data set. The integrated gene-expression data were then used for principal component analysis (PCA). Clusters were identified using shared nearest-neighbor (SNN)-based clustering using the first 30 principal components with $k = 30$ and resolution $= 0.6$. Unsupervised Uniform Manifold Approximation and Projection (UMAP) were generated from the same principal components with a minimum distance of 0.3 and 30 neighbors. This identified 18 clusters, 3 of which had a high expression for *Cd3d, Cd3e*, and *Cd3g*, constituting a total of 20,447 T cells.

T-cell clustering was performed as described above using PCA and SNN-based clustering using the first 30 components, with $k = 30$ and resolution $= 0.5$. For UMAP, a minimum distance of 0.1 was used with 20 neighbors. Ten CD8$^+$ T-cell clusters, encompassing 13,369 cells, were extracted on the basis of the exclusive expression of multiple defining genes, and reclustered as before to identify heterogeneity within these CD8$^+$ T cells.

Differential expression between clusters was performed in Seurat using "MAST," a generalized linear model created specifically for scRNA-seq data that treats cellular detection rate as a covariate. The R package monocle3 (28) was used to investigate *de novo* gene modules (genes that correlate together across cells) present within the CD8$^+$ T-cell clusters. The identity of the genes in the modules can be found in Supplementary Table S1. Using Louvain community analysis with a resolution of 0.05, differentially expressed genes (using a q value < 0.05) are clustered and grouped into modules. These modules are then compared across clusters to help inform which clusters are defined by which gene modules.

ProjecTILs T-cell classification

The mouse CD8 scRNA-seq data produced by this study were aligned to a reference tumor-infiltrating lymphocyte data set using the ProjecTILs R package (version 0.5.1; ref. 29). This data set and the subsequent program were developed using scRNA-seq data from 25 samples of melanoma, colon adenocarcinoma, and tumor-draining lymph nodes in mice resulting in 16,803 single cells for this reference atlas. A normalized expression matrix of our GIST CD8$^+$ T cells generated by Seurat version 3.0 was provided as input and additional parameters for the function "make.projection" were not changed from the default settings. Using the function "cellstate.predict," the cell state of each single cell from our data was predicted using a nearest-neighbor algorithm and then overlaid onto the UMAP of the ProjecTILs T-Cell Atlas. This analysis followed the recommended steps as described in the ProjecTILs walkthrough found at https://carmonalab.github.io/ProjecTILs.demo/tutorial.html.

IHC

IHC was performed on tumors from $Kit^{V558\Delta/+}$ mice as described previously (15) using the CD31 (Polyclonal, Abcam, cat. #ab28364) antibody. Slides were scanned with MIRAX scan (Zeiss) and analyzed with Pannoramic Viewer.

Patient samples

Tumor specimens were obtained from 20 patients with GIST who underwent surgical resection of their tumors after approval by an Institutional Review Board protocol (Supplementary Table S2). Patients provided written informed consent prior to resection, and studies were conducted in accordance with the Declaration of Helsinki. Patient information remained deidentified and encrypted in compliance with Health Insurance Portability and Accountability Act regulations. Tumor tissue was sectioned and digested at the time of collection in 5 mg/mL collagenase IV (Sigma-Aldrich, cat. #C5138-5G) and DNase I (0.5 mg/mL; Roche Diagnostics, cat. #C756V81) in HBSS for 30 minutes while shaking at 37°C. After procurement, all processed cells were immediately analyzed by flow cytometry.

Statistical analysis

Comparisons between two groups were performed using an unpaired two-tailed Student t test. Multiple group comparisons were performed using one-way ANOVA comparisons with a Bonferroni post-test for comparison of individual groups. A difference in proportion analysis was used to compare CD8$^+$ T-cell clusters from scRNA-seq. Statistics were performed on data sets using Graph Pad Prism 8.0 (Graph Pad Software). A $P < 0.05$ was considered significant. Data are shown as mean ± SEM or median.

Data availability

Bulk RNA-seq and scRNA-seq data presented in this work are submitted through the Sequencing Read Archive under accession no. PRJNA824054 and PRJNA859907. The TCRb sequencing data are available on the ImmunoSEQ platform under the project name UPenn_00110053_R-01. The remaining data generated and/or analyzed during the current study are available within the article and its Supplementary Data files or are available from the corresponding author upon reasonable request.

Results

Tumor-infiltrating CD8$^+$ T cells display a distinct phenotype in GIST

Given that chronic imatinib therapy in mouse and human GIST reduces the frequency of intratumoral TAMs and Batf3$^+$ (CD141$^+$ in humans) DCs (13, 14), we sought to determine the consequences on intratumoral CD8$^+$ T cells. We investigated tumors from $Kit^{V558\Delta/+}$ mice, which contain a point mutation in *Kit* exon 11, the most frequently affected site in human GIST. $Kit^{V558\Delta/+}$ mice develop a single imatinib-sensitive GIST in the cecum with 100% penetrance (22). Bulk RNA-seq was performed on CD8$^+$ T cells sorted from tumors, tumor-draining lymph nodes (i.e., mesenteric nodes), and spleens of 4 untreated $Kit^{V558\Delta/+}$ mice. Intratumoral CD8$^+$ T cells clustered apart from matched spleen and node CD8$^+$ T cells (**Fig. 1A** and **B**). Hallmark gene set analysis indicated that compared with

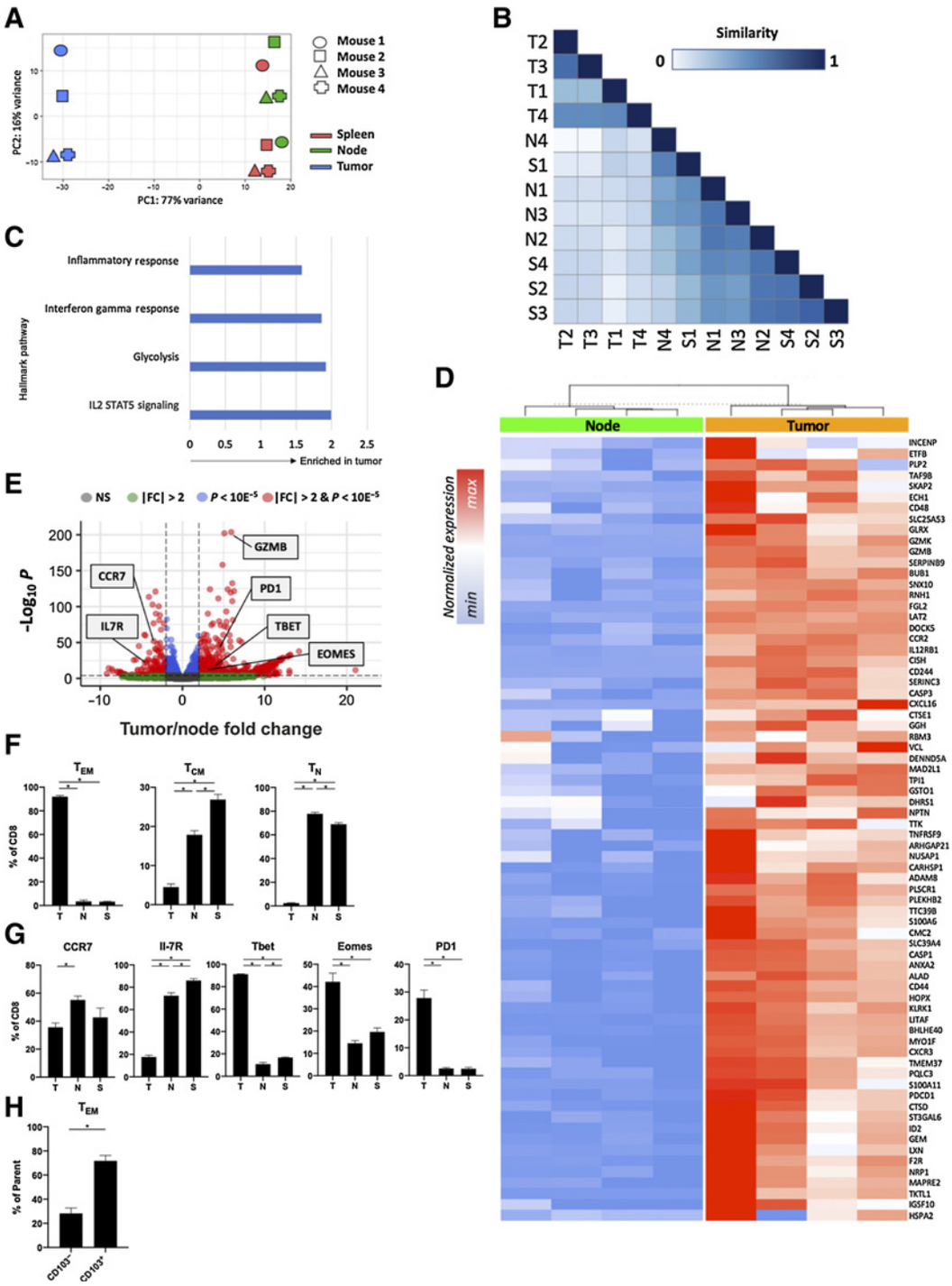

Figure 1.

Tumor-infiltrating CD8$^+$ T cells display a distinct phenotype in GIST. **A–E,** Bulk RNA-seq was performed on CD8$^+$ T cells sorted from tumors, tumor-draining lymph nodes (i.e., mesenteric nodes), and spleens of 4 untreated *KitV558*$^{\Delta/+}$ mice. **A,** PCA and (**B**) similarity of the transcriptomes of the sorted CD8$^+$ T cells from tumor (T), spleen (S), and tumor-draining lymph node (N). **C,** Hallmark inflammatory response, interferon gamma response, glycolysis, and IL2/STAT5 signaling pathway gene set enrichment (normalized enrichment score shown; all values $P < 0.05$), (**D**) heat map depicting normalized expression of select antigen response genes, and (**E**) volcano plot comparing bulk RNA-seq of the sorted CD8$^+$ T cells from *Kit*$^{V558\Delta/+}$ tumor or node. **F–H,** Flow cytometry of tumors, tumor-draining lymph nodes (i.e., mesenteric nodes), and/or spleens of untreated *KitV558*$^{\Delta/+}$ mice. **F,** Frequency of T_{EM}, T_{CM}, and T_N among CD8$^+$ T cells in tumor, spleen, or tumor-draining lymph node ($n = 4$ mice/group). **G,** Frequency of CCR7$^+$, IL7R$^+$, Tbet$^+$, Eomes$^+$, and PD-1$^+$ cells among CD8$^+$ T cells from tumors of *Kit*$^{V558\Delta/+}$ mice ($n = 4$ mice/group). **H,** Frequency of CD103$^+$ and CD103$^-$ effector CD8$^+$ T cells from tumors of *Kit*$^{V558\Delta/+}$ mice ($n = 3$ mice/group). Each column in **D** represents an individual mouse. NS, nonsignificant; FC, fold change. Data represent mean ± SEM; *, $P < 0.05$.

$CD8^+$ T cells in the tumor-draining lymph node, those in the tumor had increased inflammatory, IFNγ, and IL2/Stat5 signatures as well as increased glycolysis (**Fig. 1C**). An analysis of antigen response (**Fig. 1D**; ref. 30) and chemokine/cytokine genes (Supplementary Fig. S1A) showed higher levels of *Tnfrsf9* (i.e., 4-1BB ligand receptor), *Ccl3/4/5, Ifng*, and *Fasl* in tumor $CD8^+$ T cells. Additionally, tumor $CD8^+$ T cells had a higher expression of downstream markers of antigen response, proliferation, and cytolytic function, including *Gzmb, Pdcd1* (i.e., PD1), *Tbet*, and *Eomes* (**Fig. 1E**). In contrast, node and spleen $CD8^+$ T cells expressed more of the naïve T-cell genes *Ccr7* and *Il7r*.

We confirmed selected findings from the bulk RNA-seq analysis with flow cytometry of $CD8^+$ T cells in untreated $Kit^{V558\Delta/+}$ tumors. T_{EM} comprised 90% of all $CD8^+$ T cells, whereas the tumor-draining lymph node and spleen contained mostly T_N and T_{CM} subtypes (**Fig. 1F**; Supplementary Fig. S1B). Consistent with the bulk RNA-seq findings, tumor-draining lymph node and spleen $CD8^+$ T cells expressed CCR7 and IL7R protein, whereas tumor $CD8^+$ T cells expressed the effector/memory markers Tbet, Eomes, and PD1 (**Fig. 1G**; Supplementary Fig. S1C). We previously found that intratumoral $CD8^+CD103^-$ cells are likely antitumoral as their presence depended on $Batf3^+$ DCs, which is not the case for $CD8^+CD103^+$ cells (14). $CD103^+$ resident T cells made up about 70% of the T_{EM} population in GIST (**Fig. 1H**; Supplementary Fig. S1D). Together, these data demonstrate that tumors from $Kit^{V558\Delta/+}$ mice contain a distinct population of $CD8^+$ T cells with a predominate effector phenotype that appears more antigen-responsive and proinflammatory than those in the nearby tumor-draining lymph node or spleen.

ScRNA-seq reveals intratumoral $CD8^+$ T-cell heterogeneity

The development of high-dimensional profiling techniques such as single-cell transcriptome sequencing has allowed the field of immunology to surpass the traditional and rudimentary definitions of intratumoral $CD8^+$ T cells in both murine and human cancers (29, 31). To investigate the individual gene-expression profiles of intratumoral $CD8^+$ T cells, we performed droplet-based scRNA-seq of immune cells ($CD45^+$ cells) within $Kit^{V558\Delta/+}$ tumors. We obtained transcriptomes from 50,263 tumor-infiltrating immune cells. PCA with dimensional reduction using UMAP and unsupervised clustering identified discrete clusters of T cells, all characterized by high *Cd3e*, *Cd3g*, and *Cd3d* expression (**Fig. 2**). In untreated tumors, these T-cell clusters comprised 11,641 distinct T cells with expression of *Cd4, Cd8a*, and/or *Foxp3*, which we defined as CD4, CD8, and TReg subsets (**Fig. 2A** and **B**). Unsupervised clustering of just *Cd8a/Cd8b*-expressing cells yielded 8,065 cells separated into 10 distinct clusters (**Fig. 2C**). We then generated gene set modules that contained groups of correlated genes (Supplementary Table S1). This process resulted in 12 modules, and we used a heat map to portray how each module was enriched across the 10 clusters (**Fig. 2D**). Module 8 included the naïve T-cell markers *Ccr7, Sell, Tcf7*, and *Il7r*, which were highly expressed solely in cluster 9 (**Fig. 2E**; Supplementary Table S1). Clusters 2 and 10 coexpressed *Tcf7, Gzmb, Gzmk*, low to intermediate *Pdcd1*, and had a similar association with module 7 genes, suggesting they are T_{EM} (29). Similarly, clusters 4 and 6 both expressed high levels of granzymes and expressed *Pdcd1* and/or *Tox*, suggesting a terminally differentiated effector subtype (31, 32). Clusters 1 and 5 had low levels of naïve and effector markers and could represent an early activation subset of $CD8^+$ T cells. The resident marker *Itgae* (CD103) was expressed at an intermediate to high levels on many clusters, most notably clusters 3, 4, 6, 7, and 8, consistent with our flow cytometry findings. Overall, these data revealed that $CD8^+$ T cells in GIST exist in diverse stimulated and naïve states.

Imatinib expands intratumoral T_N and reduces T_{EM}

Once we characterized tumor $CD8^+$ T cells in untreated $Kit^{V558\Delta/+}$ mice, we determined the effects of imatinib therapy on intratumoral $CD8^+$ T cells. First, we performed bulk RNA-seq on sorted $CD8^+$ populations from $Kit^{V558\Delta/+}$ tumors, local tumor-draining lymph nodes, and spleen after vehicle or 1 week of imatinib ($n = 4$ mice/group). PCA demonstrated distinct clustering of $CD8^+$ T-cell populations based on treatment status (**Fig. 3A**). Although markers of stimulation including *Cd44* were upregulated in response to imatinib, a substantial number of effector genes were downregulated, including *Gzmb* and *Tnfrsf9* (**Fig. 3B**). There was a substantial increase in naïve T cell–signature transcripts in imatinib-treated tumors, including *Tcf7* and *Sell* (**Fig. 3B**) as well as *IL7r* (**Fig. 3C**), which were not altered in tumor-draining lymph node or spleen T cells.

Next, we performed scRNA-seq analysis of $CD8^+$ T cells from $Kit^{V558\Delta/+}$ tumors to determine the effect of 1 week of imatinib treatment on the 10 clusters. Consistent with our findings with bulk RNA-seq, there was a 4-fold increase in the proportion of cells in cluster 9, which contained the highest naïve signature (**Fig. 3D** and **E**). We also observed a relative decrease in putative effector clusters with (4 and 6) and without (5 and 10) high *Itgae* expression. Additionally, we projected our $CD8^+$ T-cell clusters onto a published reference atlas derived from murine tumors and draining lymph node from 6 studies to further identify T-cell states (**Fig. 3F**; ref. 29). The major states identified were effector memory, early activation, and naïve subsets, whereas few cells were characterized as exhausted or progenitor exhausted. The reference atlas identified a larger proportion of naïve T cells at baseline when compared with our flow cytometry results utilizing CD44 and CD62L. Naïve T cells increased in proportion after imatinib therapy, whereas effector memory and early activation T cells decreased.

To confirm our findings, we used flow cytometry to differentiate $CD8^+$ T-cell subsets after 1 and 4 weeks of imatinib treatment (Supplementary Fig. S2A). At 1 week of therapy, tumors were smaller and had a trend toward decreased T_{EM} and increased T_N cell populations, and these effects were more pronounced after 4 weeks (Supplementary Fig S2B; **Fig. 3G** and **H**). Increases in CCR7 and IL7R and decreases in Tbet and Eomes were also seen (**Fig. 3I**; Supplementary Fig. S2C). A decreased proportion of $CD8^+$ T cells in the tumor was found at 1 and 4 weeks of imatinib therapy, but this change did not appear to be due to increased apoptosis of $CD8^+$ T cells (Supplementary Fig. S2D and S2E). Within the T_{EM} subset, there was stable PD1 protein expression at 1 week that decreased by 4 weeks, indicating less differentiation and stimulation over time (**Fig. 3J**). Consistent with our prior work (14), the T_N population at 1 and 4 weeks of imatinib therapy consisted almost entirely of $CD103^-CD8^+$ T cells (**Fig. 3K**), suggesting they were derived peripherally. We considered whether older $Kit^{V558\Delta/+}$ mice had altered $CD8^+$ T-cell subsets at baseline compared with younger mice but found no difference (Supplementary Fig. S2F). Additionally, CD31 staining was similar in tumors with and without 4 weeks of imatinib therapy, indicating that the increased T_N population was not due to increased tumor vascularity (Supplementary Fig. S2G). Collectively, these data indicated that imatinib therapy causes a phenotypic shift from T_{EM} to T_N in the tumor microenvironment, particularly with a longer time of treatment.

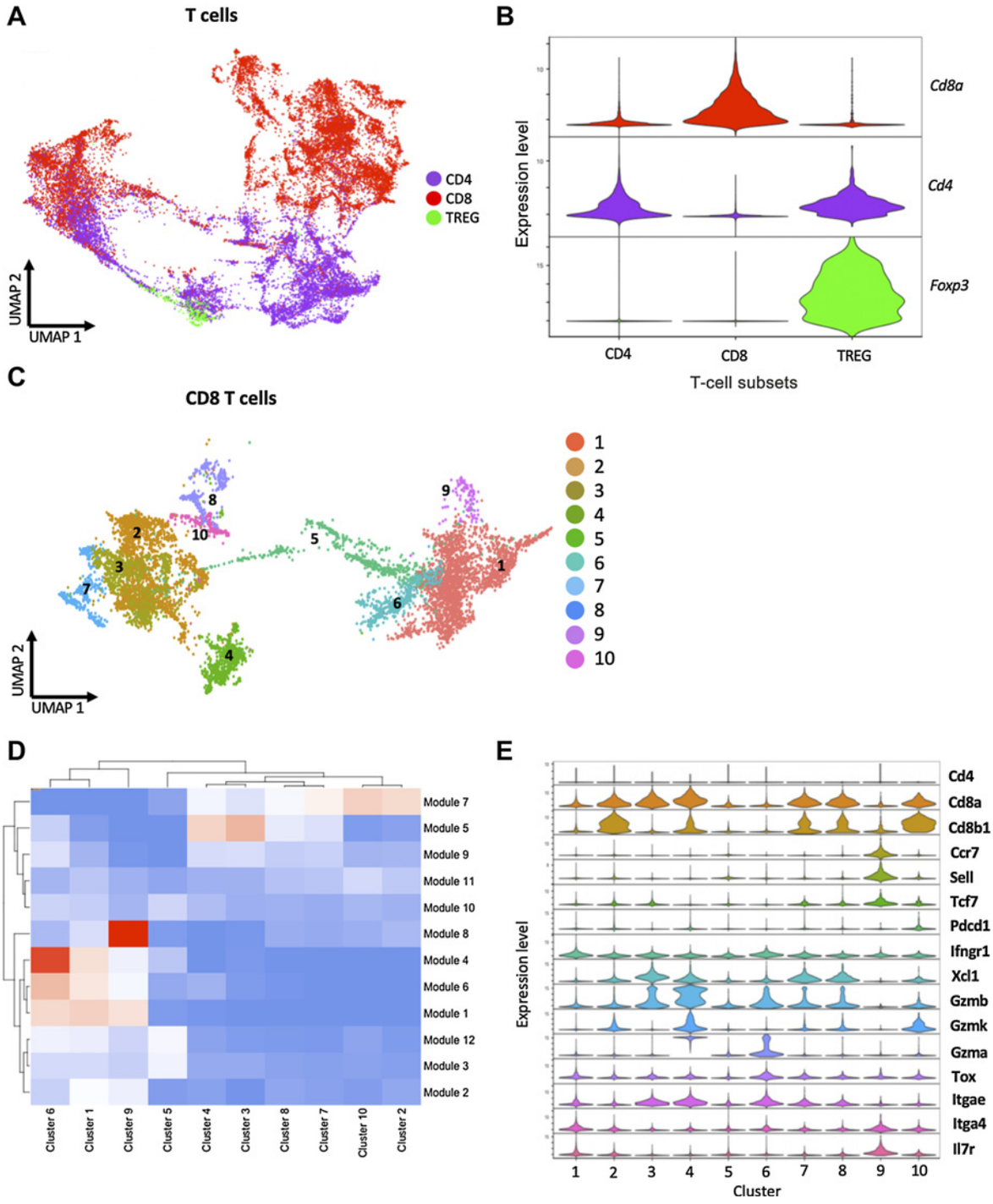

Figure 2.

ScRNA-seq reveals intratumoral CD8$^+$ T-cell heterogeneity. Droplet-based scRNA-seq was performed on immune cells (CD45$^+$ cells) sorted from tumors from 3 untreated *KitV558*$^{\Delta/+}$ mice. **A,** Clusters of CD4$^+$ T cells, CD8$^+$ T cells, and Tregs within the CD3$^+$ compartment based on unsupervised clustering by PCA, defined by (**B**) *cd4, cd8a*, and *foxp3* expression. **C,** Numbered clusters within the intratumoral CD8$^+$ T-cell compartment based on unsupervised clustering by PCA. **D,** Heat map of gene-expression modules, with stratified module enrichment by CD8$^+$ T-cell clusters. **E,** Violin plots of expression of select genes in CD8$^+$ T-cell clusters. **A** and **C,** UMAP plots display scRNA-seq profiling of 11,641 *cd3d/e/g* and 8,065 *cd8a/b* T cells from 3 mice as detailed in the methods section.

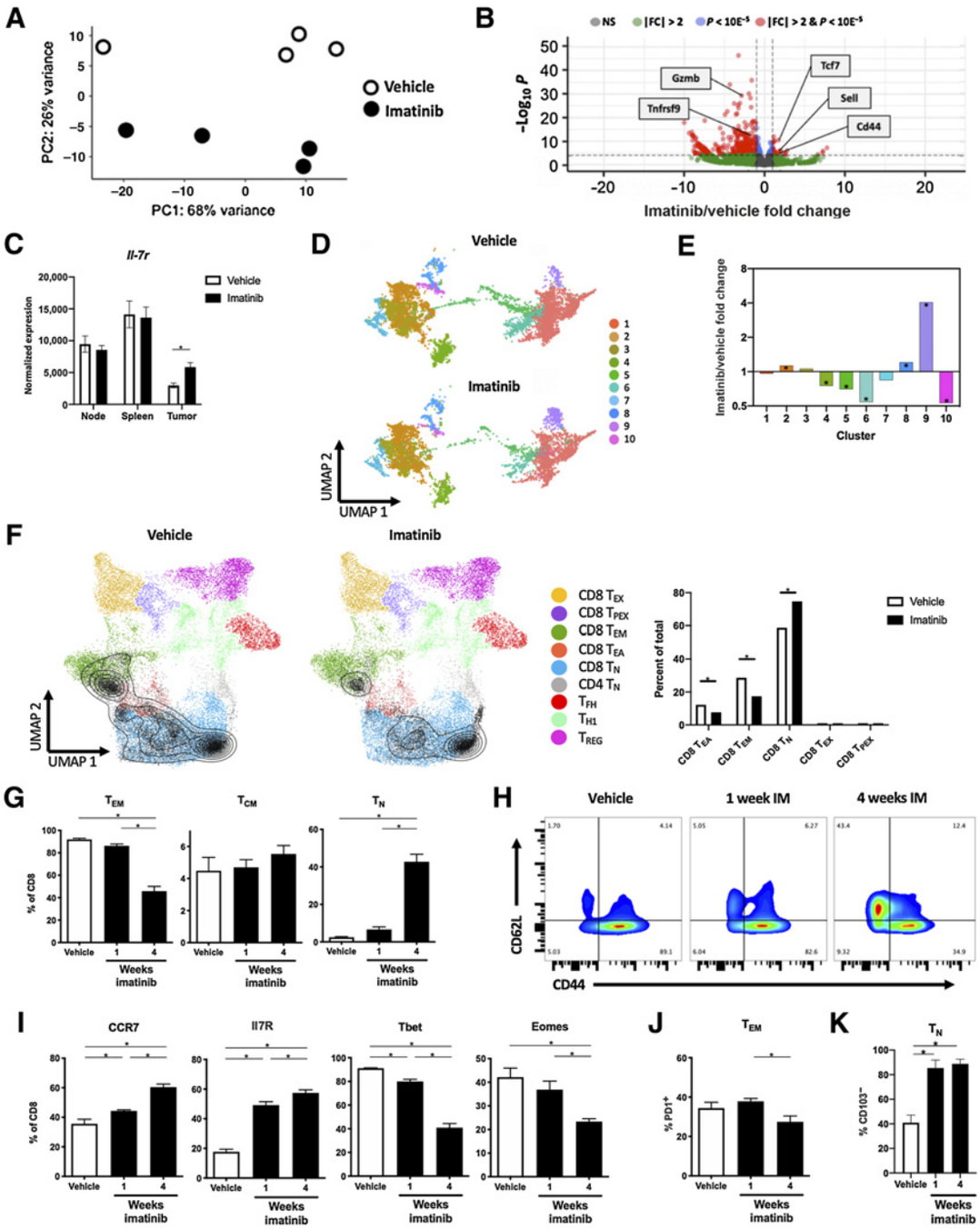

Figure 3.

Imatinib expands intratumoral T_N and reduces T_{EM}. **A–C,** $Kit^{V558\Delta/+}$ mice were treated with vehicle or imatinib for 1 week ($n = 4$ mice/group). At that time, tumors, tumor-draining lymph nodes (i.e., mesenteric nodes), and spleens were harvested and bulk RNA-seq was performed on $CD8^+$ T cells sorted from the tissues. **A,** PCA and (**B**) volcano plot of sorted $CD8^+$ T cells from tumor. **C,** Normalized expression of *Il7r* in node, spleen, or tumor. Each point in **A** represents a sample from an individual mouse. **D** and **E,** $Kit^{V558\Delta/+}$ mice were treated with vehicle or imatinib for 1 week ($n = 3$ mice/group). At that time, scRNA-seq was performed on $CD45^+$ cells sorted from the tumors. **D,** UMAP plot of $CD8^+$ T-cell clusters and (**E**) cluster imatinib/vehicle fold change in tumors. **F,** $CD8^+$ T-cell clusters from (**D**), represented as gray triangles/isobars were projected onto a published reference atlas (29) and the difference in the proportion of T-cell states including exhausted (T_{EX}), precursor exhausted (T_{PEX}), T_{EM}, early activation (T_{EA}), and T_N were compared between vehicle and imatinib groups. **G–J,** $Kit^{V558\Delta/+}$ mice were divided into 3 groups on day 0, and all mice were sacrificed on day 28. Mice were treated with vehicle or imatinib for 1 or 4 weeks, and tumors were analyzed by flow cytometry for (**G**) frequency of T_{EM}, T_{CM}, and T_N among $CD8^+$ T cells; (**H**) $CD44^+$ and $CD62L^+$ expression in $CD8^+$ T cells; (**I**) frequency of $CCR7^+$, $IL7R^+$, $Tbet^+$, $Eomes^+$ cells among $CD8^+$ T cells; (**J**) frequency of $PD1^+$ cells among T_{EM} $CD8^+$ T cells; and (**K**) frequency of $CD103^-$ T_N cells among $CD8^+$ T cells ($n = 3$–4 mice/group). Data represent mean ± SEM; *, $P < 0.05$.

Imatinib restricts PI3K signaling and clonal expansion in intratumoral CD8$^+$ T cells

To identify the mechanism of the phenotypic shift from T_{EM} to T_N in GIST following imatinib therapy, we first examined our bulk RNA-seq data. Hallmark gene analysis established that CD8$^+$ T cells in imatinib-treated tumors at 1 week had many downregulated pathways related to T-cell stimulation, inflammation, and proliferation compared with controls (**Fig. 4A**). Bulk RNA-seq demonstrated that *Pdcd1* was upregulated (**Fig. 4B**), which we suspect was a result of transient stimulation of CD8$^+$ T cells due to a decrease in IDO, which we found previously (12). We found that changes in the CD8$^+$ T-cell subsets coincided with alterations in chemokine production by the tumor. On bulk RNA-seq of tumors and sorted CD8$^+$ populations, most chemokines in the tumor were decreased after imatinib treatment, whereas the majority of their complementary receptors were increased in CD8$^+$ T cells (Supplementary Fig. S3A and S3B). One chemokine that increased after treatment was *Ccl21*, which binds Ccr7 and recruits naïve T cells (33). To test whether imatinib therapy affected the recruitment of CD8$^+$ T cells into the tumor, following CD8$^+$ T-cell depletion, we adoptively transferred CSFE-labeled CD8$^+$ T cells from CD45.1 mice into $Kit^{V558\Delta/+}$ mice receiving imatinib therapy. We found significantly fewer CD45.1$^+$CSFE$^+$CD8$^+$ T cells per gram of tumor in $Kit^{V558\Delta/+}$ mice receiving imatinib compared with controls, whereas the proportion of CD45.1$^+$CSFE$^+$CD8$^+$ T cells in the spleen was similar between the two groups (**Fig. 4C**).

Our previous work demonstrated that imatinib therapy caused both an M1 to M2 transition of intratumoral macrophages as well as depletion of Batf3$^+$ DCs (13, 14), so we suspected that decreased antigen presentation and/or costimulation contributed to intratumoral CD8$^+$ naivety following imatinib treatment. To explore this, we assessed TCR and/or CD28 costimulation by measuring downstream PI3K signaling, as others have done (34). First, we used our bulk RNA-seq data to evaluate *Akt* and *mTor* transcription in imatinib-treated tumors, which showed no difference compared with controls (**Fig. 4D**). By flow cytometry, tumor CD8$^+$ T cells had higher baseline levels of p-Akt and p-mTor compared with CD8$^+$ T cells from tumor-draining lymph node, and imatinib decreased phosphorylation, signifying a reduction in PI3K signaling (**Fig. 4E**). To determine whether imatinib had a direct effect on CD8$^+$ T cells, isolated splenic CD8$^+$ T cells were cultured in the presence of CD3/CD28 beads with or without imatinib, which demonstrated no difference in p-AKT and p-mTOR median fluorescence intensity (MFI; Supplementary Fig. S3C). There was, however, decreased transcription of the scaffold adaptor for PI3K (*Pik3ap1*; Supplementary Fig. S3D), which is critical for propagating CD8$^+$ T-cell PI3K signaling and clonal expansion (35).

Next, we assessed TCR cell clonal expansion in matched $Kit^{V558\Delta/+}$ tumors, spleen, and cecum by ImmunoSEQ assay (Adaptive Biotechnologies). There was a trend toward more unique productive TCR sequences in spleen CD8$^+$ T cells than in tumor or cecum CD8$^+$ T cells at baseline, and this difference was significant following imatinib treatment (**Fig. 4F**). The occupied repertoire space of large and hyperexpanded clonotypes was unchanged after treatment, as was clonality, as indicated by Simpson clonality (**Fig. 4G**; Supplementary Fig. S3E), indicating a lack of TCR clonal expansion. TCRs were very similar in tumor and cecum from the same mouse, and TCRs in untreated tumors were similar at baseline and after imatinib treatment (Supplementary Fig. S3F). Thus, intratumoral CD8$^+$ T cells have diminished chemokine and PI3K signaling and lack clonal expansion following imatinib therapy, supporting the hypothesis that both recruitment and deficiency of antigen presentation/costimulation contribute to the changes in the CD8$^+$ T-cell subsets following imatinib therapy.

Human GIST display differential CD8$^+$ T-cell subsets

To determine the clinical relevance of our findings from $Kit^{V558\Delta/+}$ mice, we performed flow cytometry on 20 freshly obtained GIST specimens from 20 patients (Supplementary Table S2). Tumors were classified as untreated, sensitive, or resistant to imatinib at the time of surgery based on serial radiologic assessment, as described previously (12). Because we found that the T_{EM} and T_N populations in murine GIST were significantly altered in imatinib-treated tumors, we first evaluated the expression of the human naïve/memory markers CD45RA and CD45RO. We found that the proportion of CD45RA$^+$CD45RO$^-$CD8$^+$ T cells was significantly increased in sensitive tumors after a median of 12 months of imatinib treatment (**Fig. 5A**; Supplementary Fig. S4). Further analysis of the CD8$^+$ T_N (CD45RA$^+$CCR7$^+$), T_{CM} (CD45RA$^-$CCR7$^+$), T_{EM} (CD45RA$^-$CCR7$^-$), and effector memory cells reexpressing CD45RA (T_{EMRA}, CD45RA$^+$CCR7$^-$) showed that the abundance of T_N and T_{EM} cells was higher and lower, respectively, between the untreated and sensitive groups (**Fig. 5B**). These changes were not present in the resistant group. There was an increase in terminally differentiated T_{EMRA} cells in the sensitive group compared with the untreated group, indicating that the sensitive group had a terminally differentiated CD8$^+$ T-cell subset of uncertain proliferative potential (36, 37). Overall, sensitive human GISTs had a lower and higher proportion of T_{EM} and T_N CD8$^+$ T cells compared with untreated GIST.

IL15-mediated stimulation with ICB improves the response to imatinib

Given the seemingly negative effects of imatinib on intratumoral CD8$^+$ T cells, particularly after longer treatment times, we investigated methods to improve the antitumoral immune response. We considered stimulation with IL15 given its known influence on the PI3K pathway in T cells (38) and because it was most highly expressed by intratumoral Batf3$^+$ DCs by scRNA-seq, and these cells are reduced with imatinib (Supplementary Fig. S5A; ref. 14). We investigated which of our scRNA-seq CD8$^+$ clusters expressed *Il2rb* and *Il2rg*, which comprise the heterodimer required for IL15 signaling. Although *Il2rg* expression was similar among all clusters, *Il2rb* was highly expressed in the effector cluster 6 and expressed at the lowest level in the naïve cluster 9 (Supplementary Fig. S5B). Hence, we speculated that IL15 may preferentially propagate an effector T-cell response. The IL15/IL15Rα superagonist (IL15SA) has been demonstrated to increase the half-life of IL15 and support naïve and memory CD8$^+$ T-cell proliferation, and new formulations have been used with limited side effects in early clinical trials (39, 40). Therefore, we treated $Kit^{V558\Delta/+}$ mice with imatinib and IL15SA for 1 week (**Fig. 6A**). At 1 week, there were additive effects of IL15SA with imatinib therapy, as tumors weighed 30% less than after treatment with imatinib alone (**Fig. 6B**; Supplementary Fig. S5C). IL15SA therapy alone did not reduce tumor size (Supplementary Fig. S5D). There was a similar histologic appearance of the tumors among treatment groups (Supplementary Fig. S5E). We also considered the effect of IL15SA on natural killer (NK) cells, as they express *Il2rb* in GIST (Supplementary Fig. S5F). However, NK cells are infrequent in GIST, did not expand after treatment with imatinib and IL15SA compared with imatinib alone (Supplementary Fig. S5G), and as we showed previously, NK-cell depletion in $Kit^{V558\Delta/+}$ mice does not affect tumor size (12). Combination therapy increased T_{EM} compared with imatinib

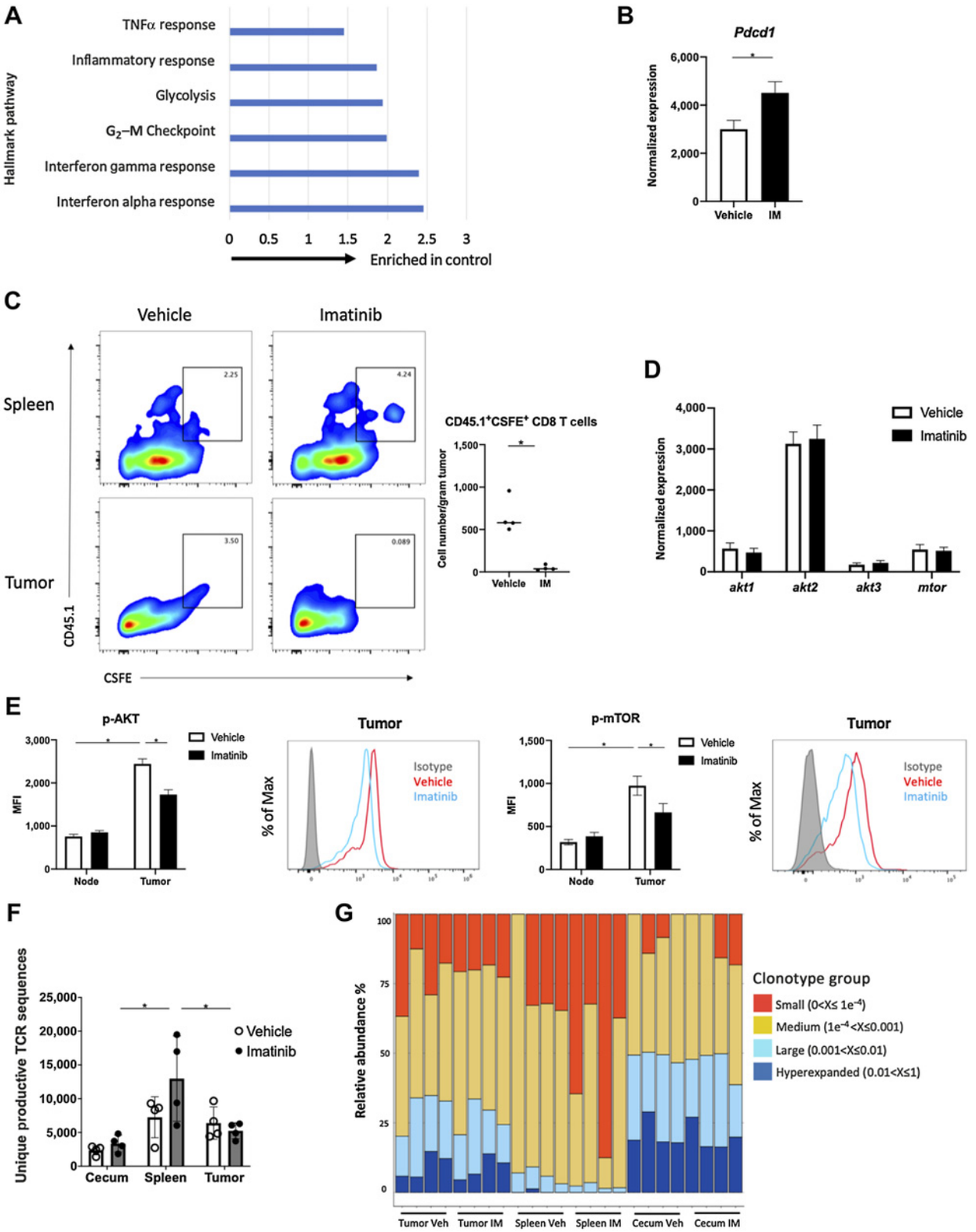

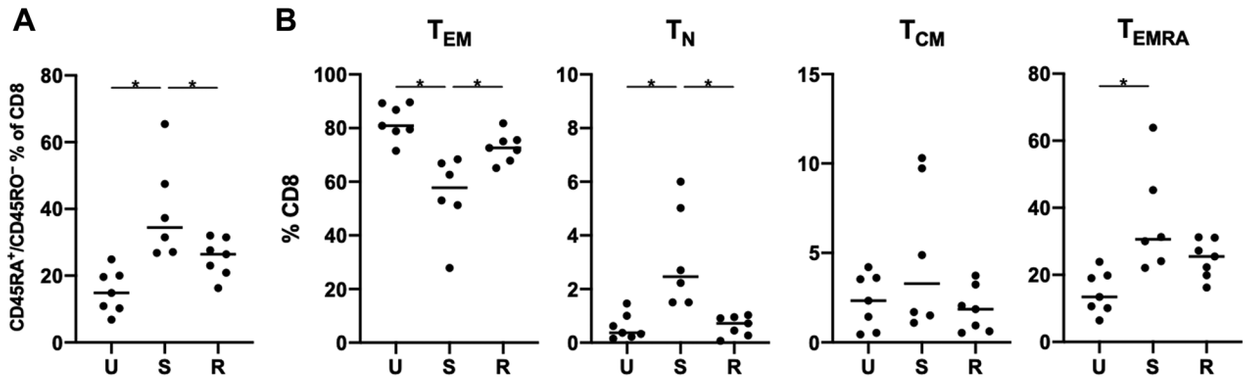

Figure 5.
Human GIST display differential CD8$^+$ T-cell subsets. CD8$^+$ T cells from human GIST specimens (20 tumor specimens from 20 patients) were analyzed by flow cytometry for (**A**) frequency of CD45RA and CD45RO expression among CD8$^+$ T cells and (**B**) frequency of memory subsets among the CD8$^+$ T-cell population. Line indicates median; *, $P < 0.05$

alone and blunted the increase in T_N induced by imatinib (**Fig. 6C**; Supplementary Fig. S5H).

Because we found that imatinib therapy decreased Akt and mTor signaling in intratumoral CD8$^+$ T cells, we investigated the effect of IL15SA combination therapy on the PI3K pathway. Adding IL15SA to imatinib therapy fully restored CD8$^+$ T-cell p-Akt and partially restored p-mTor expression by flow cytometry (**Fig. 6D**). To determine whether the antitumor effects of imatinib and IL15SA combination therapy depended on CD8$^+$ T cells, we used an antibody to deplete the CD8$^+$ cells. This abrogated the benefit of adding IL15SA during imatinib therapy as there was no incremental change in tumor weight and CD8$^+$ T cells remained significantly depleted despite IL15SA therapy (**Fig. 6E**; Supplementary Fig. S5I). Further, we sought to test the effect on imatinib therapy of Il15SA, ICB, or both IL15SA and ICB, particularly at longer time points. Although tumors treated with IL15SA and imatinib for 4 weeks were smaller than those treated with imatinib alone (**Fig. 6F**), the proportion of intratumoral T_{EM} was not increased as was seen at 1 week of therapy, possibly due to tachyphylaxis. Combined therapy using IL15SA and anti–PD-1 with imatinib increased the proportion of intratumoral T_{EM} and decreased T_N at 4 weeks (**Fig. 6G**; Supplementary Fig. S5J), as well as had the greatest tumor killing. Consistent with these findings, triple therapy resulted in the highest proportion of CD8$^+$ T cells expressing Ki67 and granzyme B at 4 weeks of treatment (**Fig. 6G**; Supplementary Fig. S5K). Therefore, treatment of GIST with imatinib and IL15SA improved tumor response and rescued PI3K signaling in CD8$^+$ T cells at an early time point. Combination therapy with IL15SA and ICB was needed to maximize tumor killing and effector CD8$^+$ T-cell subsets for longer durations of therapy.

Discussion

We investigated the molecular signatures of intratumoral CD8$^+$ T cells in *Kit*$^{V558\Delta/+}$ mice at the single-cell level. We found that CD8$^+$ T cells in GIST have a distinctive molecular profile consistent with an effector phenotype and cytotoxic ability compared with matched CD8$^+$ T cells from secondary lymphoid organs. CD8$^+$ T cells from the local lymph node were more similar to CD8$^+$ T cells from the spleen than the tumor. These findings suggest that there may not be communication between the tumor and draining lymph node, which is consistent with the fact that GISTs, like most sarcomas, do not metastasize to lymph nodes. Our TCR sequencing results support the existence of tumor-specific antigens, as the relative abundance of hyperexpanded TCR clones was higher in untreated tumors, where there are more mature CD8$^+$ T cells compared with spleen. Immunogenic antigens have not been identified in GIST, although mutant KIT or PDGFRA peptides are attractive possibilities. We previously estimated that the majority of patients with an oncogenic mutation in *PDGFRA* or *KIT* produced at least one high-affinity neoepitope (16). That TCR sequences were similar between cecum and tumor suggests that T cells from the surrounding intestine infiltrate GIST. Despite the

Figure 4.
Intratumoral CD8$^+$ T cells have restricted PI3K signaling and lack clonal expansion in response to imatinib. **A** and **B,** *Kit*$^{V558\Delta/+}$ mice were treated with vehicle or imatinib for 1 week ($n = 4$ mice/group) and sorted CD8$^+$ T cells from tumors were analyzed by bulk RNA-seq for (**A**) hallmark TNF alpha response, inflammatory response, glycolysis, G_2–M checkpoint, interferon gamma response, and interferon alpha response gene set enrichment (normalized enrichment score shown; all values $P < 0.05$); and (**B**) *Pdcd1* expression. **C,** Following CD8$^+$ T-cell depletion with one dose of anti-CD8 on day 0, *Kit*$^{V558\Delta/+}$ mice were treated with vehicle or imatinib for 5 days. On day 4, mice received CSFE-labeled splenic CD8$^+$ T cells from congenic CD45.1 mice by adoptive transfer. On day 5, the frequency of CSFE$^+$CD45.1$^+$CD8$^+$ T cells in the spleen and tumor was determined by flow cytometry, as well as the cell count in the tumor ($n = 4$ mice/group, pooled from two independent experiments). **D,** Normalized expression of *Akt1, Akt2, Akt3*, and *Mtor* in sorted CD8$^+$ T cells in tumors from *Kit*$^{V558\Delta/+}$ mice following bulk RNA-seq, as in **A** and **B** ($n = 4$ mice/group). **E,** Median fluorescence intensity (MFI) and representative histograms of p-AKT$^+$ and p-mTOR$^+$ cells among CD45$^+$CD3$^+$NK1.1$^-$CD4$^-$CD8$^+$ T cells in tumor and tumor-draining lymph node from untreated *Kit*$^{V558\Delta/+}$ mice (5 mice/group, repeated twice). **F** and **G,** *Kit*$^{V558\Delta/+}$ mice were treated with vehicle (Veh) or imatinib (IM) for 1 week ($n = 4$ mice/group). At that time, tumors, spleens, and cecum were harvested and analyzed by high-throughput sequencing of the CDR3 TCRβ region. **F,** Unique productive TCR sequences and (**G**) occupied repertoire space of small, medium, large, and hyperexpanded clonotype groups where units represent clonal frequency. Data represent mean ± SEM; *, $P < 0.05$.

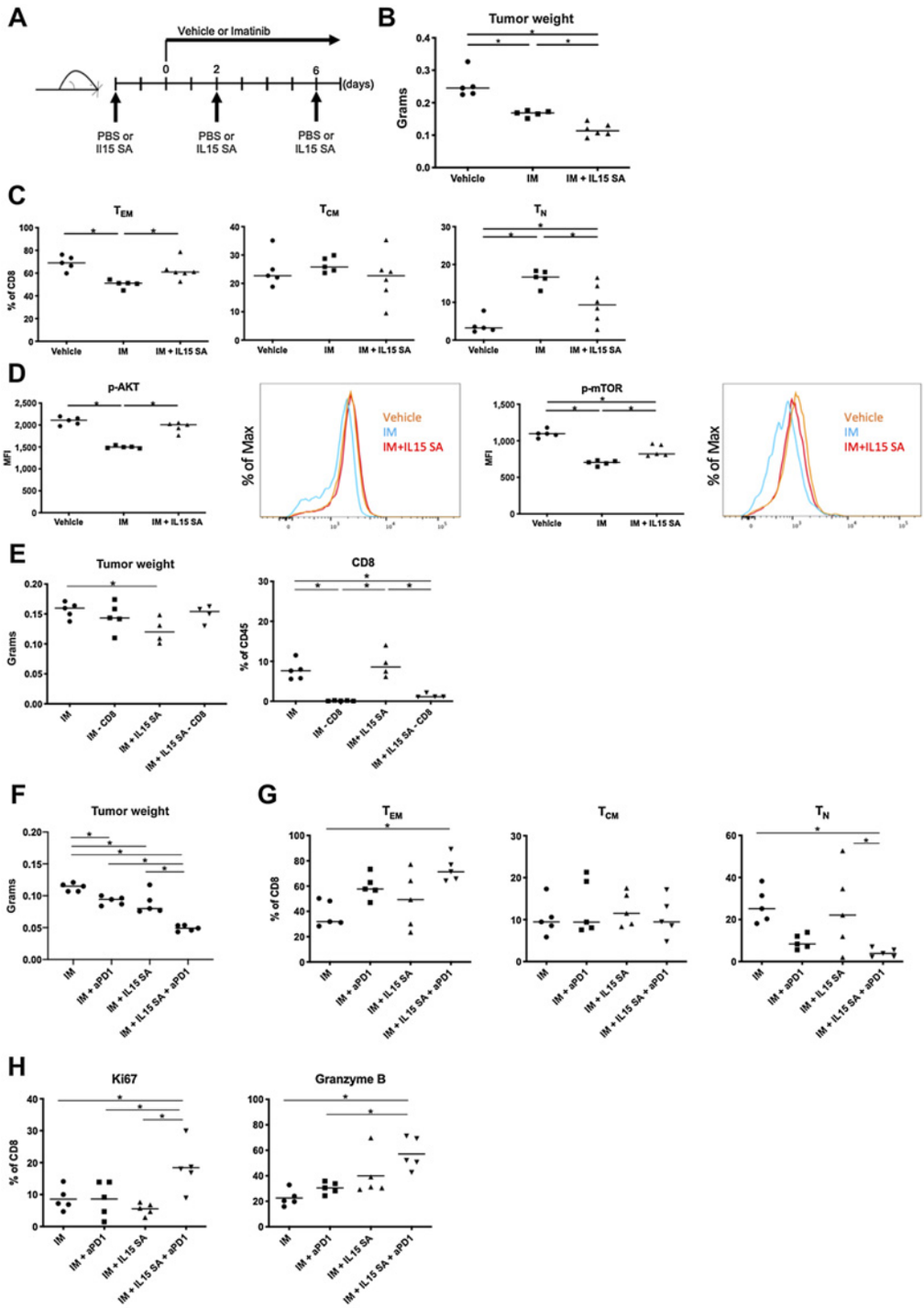

Figure 6.

IL15-mediated stimulation with immune-checkpoint blockade improves the response to imatinib. **A,** $Kit^{V558\Delta/+}$ mice were treated with IL15SA three times over the course of 9 days and given imatinib daily for 7 days. Controls received PBS for 9 days and vehicle or imatinib from days 0 to 7. **B,** Tumor weights of $Kit^{V558\Delta/+}$ GIST treated as described in **A** ($n = 5$–6 mice/group, repeated twice). Flow cytometry of tumors was performed to determine (**C**) frequency of T_{EM}, T_{CM}, and T_N among intratumoral $CD8^+$ T cells and (**D**) MFI and representative histogram of p-AKT^+ or p-$mTOR^+$ $CD8^+$ T cells in tumors from $Kit^{V558\Delta/+}$ mice ($n = 5$ mice/group, repeated twice). **E,** $Kit^{V558\Delta/+}$ mice were treated with IM (imatinib), IM + depleting anti-CD8 (-CD8), IM + IL15SA, or IM + IL15SA + -CD8 and assessed for tumor weight and frequency of $CD8^+$ T cells among $CD45^+$ cells, as assessed by flow cytometry (4–5 mice/group). **F,** $Kit^{V558\Delta/+}$ mice were treated with IM, IM + aPD1 (anti–PD-1), IM + IL15SA, or IM + IL15SA + aPD1 for 4 weeks and assessed for tumor weight (5 mice/group, pooled from two independent experiments). Flow cytometry was used to assess these mice for (**G**) $CD8^+$ T-cell subsets and (**H**) frequency of $Ki67^+$ and granzyme B^+ cells among $CD8^+$ T. Line indicates median; *, $P < 0.05$.

immunogenicity of intratumoral CD8$^+$ T cells and their activation following IDO inhibition with imatinib (12), they did not appear to undergo clonal expansion. Overall, our findings highlight the limitation of using imatinib as a sole immune modulator.

The present data build on our previous work (12–14, 41) demonstrating the widespread effects of imatinib on the tumor immune microenvironment. Here, we have further investigated the effects of this TKI on intratumoral CD8$^+$ T cells with respect to naïve and effector subsets, gene expression at the bulk and single-cell levels, and TCR phenotype. Our previous work investigated the effect of IDO inhibition through imatinib treatment on CD8$^+$ T-cell functionality at a short time point (1 week), whereas here we have discovered that chronic (4 weeks) imatinib therapy increases the proportion of naïve CD8$^+$ T cells within the tumor in our mouse model of GIST, which may have major implications for the combined use of TKIs and immunotherapy. To attempt to maximize the antitumor effect of CD8$^+$ T cells during imatinib therapy, we treated GIST with imatinib and IL15SA therapy, with or without concomitant anti–PD-1 therapy.

The immune response and its modulation by TKI treatment in GIST is complex. Utilizing scRNA-seq in our mouse model of GIST allowed a unique view into the early effects of imatinib on molecularly defined CD8$^+$ T-cell subsets. scRNA-seq in melanoma responsive to PD1 blockade has demonstrated the clonal replacement of CD8$^+$ T cells by newly infiltrating T cells (41). In keeping with our integration method of scRNA-seq, we did not find a discrete CD8$^+$ T-cell cluster solely defined by either vehicle or imatinib-treated cells in our model. Rather, we observed a shift in the relative frequencies of our defined clusters, which mimicked our flow cytometry data. We also saw a similar shift in T-cell subsets when analyzing a previously published reference atlas (29). scRNA-seq is revealing the intricacies of the tumor immune response and challenging decades of research using traditional techniques. One study used scRNA-seq to associate T-cell states in primary human melanoma and metastatic lymph nodes to checkpoint blockade response. Through this analysis (42) and others (29), these authors concluded that tumor-infiltrating lymphocytes (TIL) expressing TCF7, and not conventional markers of tumor response including PD1, were enriched in responders versus nonresponders both pre- and posttreatment. Furthermore, when TILs from primary melanoma and metastatic lymph node were projected onto a T-cell reference atlas of 25 scRNA-seq samples from six studies, responders had a relative 2- to 4-fold increase in naïve CD4$^+$ and CD8$^+$ T cells compared with nonresponders (29). In our study, we suspected that the naïve CD8$^+$ T-cell infiltrate following imatinib limited an effective immune response. However, it is evident that predictors of response to immunotherapy are both tumor- and agent-specific. To further investigate the potential interaction of our CD8$^+$ T-cell clusters within the tumor immune environment, we plan to apply the novel technique of spatially resolved transcriptomics, which is beyond the scope of this report.

There have been few studies evaluating TILs in human GIST, but the presence of TILs has been positively correlated with PFS (43). We previously reported that effector CD8$^+$CD45RO$^+$CCR7$^-$ T cells are enriched in GIST compared with matched blood, and PD-L1 is expressed in GIST but reduced with imatinib (14, 15). Others have compared GIST to various sarcomas and found that GISTs have a high number of infiltrating CD8$^+$ T cells comprised mostly of T_{EM} and T_{EMRA} subtypes, consistent with our findings (44). GIST also has lower expression of costimulatory ligands and a higher polyclonal T-cell repertoire compared with other sarcomas, with 5 of 9 GISTs in this study having received imatinib (44). Tumor mutational burden (TMB) has recently been used to predict response to immunotherapy. However, TMB may not be a useful marker in GIST, which is typically driven by a single mutation and has a low TMB of 1.8 mutations/megabase (45). In fact, GIST, and other tumors driven by activating mutations, may prove to be an exception to the normal relationship between TMB and immune response (46). There have been no studies using TMB to evaluate immunotherapy response in GIST. In addition, TMB will need to be validated as a predictor of response to immunotherapy when combined with targeted molecular agents such as TKIs (47).

Imatinib has changed the standard of care for patients with GIST in both the adjuvant and neoadjuvant setting, and it has prolonged median survival in advanced GIST from a historical 16 to 19 months to 5 years (3, 48). The interpretation of our human data is limited because patients with imatinib-sensitive GISTs in this study had already been treated with the TKI for a median of 12 months. Furthermore, we cannot determine whether the observed changes in CD8$^+$ T-cell subsets were directly related to imatinib therapy. Nonetheless, there were correlations in the changes of T_N and T_{EM} in tumors of $Kit^{V558\Delta/+}$ mice and sensitive human GIST. CD8$^+$ T cells in patients with resistant GIST (progressing at the time of surgery despite being treated with a TKI) reverted to levels seen in untreated GISTs, emphasizing the central role of oncogenic signaling in GIST. Given imatinib's broad impact, we venture whether the future of GIST treatment and other cancers treated with TKIs lies in alternating immunotherapy with TKIs in order to maximize the benefit of both therapies.

Historically, T-cell agonism in cancer therapy was achieved with IL2, which induced durable responses in patients with metastatic melanoma and renal cell carcinoma, albeit with some toxicity (49). Recombinant IL15 has also been trialed, but due to the variable expression of IL15R, which acts to stabilize and increase the biological activity of IL15, high doses were required to achieve responses (50). The IL15SA ALT-803 has been tested in patients as a monotherapy and in combination with PD1 and CTLA-4 checkpoint blockade (40, 51, 52). ALT-803 alone increased circulating NK and CD8$^+$ T cells, as well as Ki-67 expression on CD8$^+$ T cells (40). In a study of non–small cell lung cancer (52), ALT-803 induced objective responses after treatment relapse or failure following anti–PD-1 immunotherapy. The same group also found that ALT-803 decreased the clonality of peripheral TCRs, which could imply an increase in neoantigen-reactive T cells. We found a decrease in clonality in our spleen samples following imatinib treatment, suggesting imatinib could have a similar effect. In addition, we found that IL15SA therapy in GIST had a pan-CD8$^+$ T-cell effect despite our hypothesis that it would preferentially augment effector cells. This finding may be beneficial in GIST, as imatinib alters the relative frequencies of CD8$^+$ T cells, including decreasing the T_{EM} population. Collectively, our results provide the rationale for including an IL15SA in addition to checkpoint blockade in future trials of GIST.

Authors' Disclosures

R.P. DeMatteo reports grants from Blueprint Medicines. No disclosures were reported by the other authors.

Authors' Contributions

A.D. Tieniber: Conceptualization, data curation, formal analysis, validation, investigation, methodology, writing–original draft, writing–review and editing. **A.N. Hanna:** Conceptualization, data curation, formal analysis, validation, writing–review and editing. **B.D. Medina:** Conceptualization, data curation, formal analysis, methodology, writing–review and editing. **G.A. Vitiello:** Data curation, formal analysis, writing–review and editing. **M.S. Etherington:** Data curation, formal

analysis. **M. Liu:** Data curation, formal analysis. **K.J. Do:** Data curation, validation. **F. Rossi:** Supervision, funding acquisition. **R.P. DeMatteo:** Conceptualization, resources, supervision, funding acquisition, writing–original draft, project administration, writing–review and editing.

Acknowledgments

The investigators were supported by NIH grants R01 CA102613 and T32 CA251063, the David Foundation, Betsy Levine-Brown and Marc Brown, and the GIST Cancer Research Fund (R.P. DeMatteo). The authors are grateful for the assistance of the Office of Laboratory Animal Welfare, University Laboratory Animal Resources, and flow cytometry staff at the University of Pennsylvania.

The costs of publication of this article were defrayed in part by the payment of page charges. This article must therefore be hereby marked *advertisement* in accordance with 18 U.S.C. Section 1734 solely to indicate this fact.

Note

Supplementary data for this article are available at Cancer Immunology Research Online (http://cancerimmunolres.aacrjournals.org/).

Received December 2, 2021; revised April 7, 2022; accepted July 27, 2022; published first August 2, 2022.

References

1. Mastrangelo G, Coindre JM, Ducimetière F, Dei Tos AP, Fadda E, Blay JY, et al. Incidence of soft tissue sarcoma and beyond: a population-based prospective study in 3 European regions. Cancer 2012;118:5339–48.
2. Joensuu H, DeMatteo RP. The management of gastrointestinal stromal tumors: a model for targeted and multidisciplinary therapy of malignancy. Annu Rev Med 2012;63:247–58.
3. Blanke CD, Demetri GD, von Mehren M, Heinrich MC, Eisenberg B, Fletcher JA, et al. Long-term results from a randomized phase II trial of standard- versus higher-dose imatinib mesylate for patients with unresectable or metastatic gastrointestinal stromal tumors expressing KIT. J Clin Oncol 2008;26:620–5.
4. Demetri GD, von Mehren M, Blanke CD, Van den Abbeele AD, Eisenberg B, Roberts PJ, et al. Efficacy and safety of imatinib mesylate in advanced gastrointestinal stromal tumors. N Engl J Med 2002;347:472–80.
5. Gold JS, van der Zwan SM, Gonen M, Maki RG, Singer S, Brennan MF, et al. Outcome of metastatic GIST in the era before tyrosine kinase inhibitors. Ann Surg Oncol 2007;14:134–42.
6. Verweij J, Casali PG, Zalcberg J, LeCesne A, Reichardt P, Blay JY, et al. Progression-free survival in gastrointestinal stromal tumours with high-dose imatinib: randomised trial. Lancet 2004;364:1127–34.
7. Blanke CD, Rankin C, Demetri GD, Ryan CW, von Mehren M, Benjamin RS, et al. Phase III randomized, intergroup trial assessing imatinib mesylate at two dose levels in patients with unresectable or metastatic gastrointestinal stromal tumors expressing the kit receptor tyrosine kinase: S0033. J Clin Oncol 2008;26:626–32.
8. Antonescu CR, Besmer P, Guo T, Arkun K, Hom G, Koryotowski B, et al. Acquired resistance to imatinib in gastrointestinal stromal tumor occurs through secondary gene mutation. Clin Cancer Res 2005;11:4182–90.
9. Demetri GD, van Oosterom AT, Garrett CR, Blackstein ME, Shah MH, Verweij J, et al. Efficacy and safety of sunitinib in patients with advanced gastrointestinal stromal tumour after failure of imatinib: a randomised controlled trial. Lancet 2006;368:1329–38.
10. Demetri GD, Reichardt P, Kang YK, Blay JY, Rutkowski P, Gelderblom H, et al. Efficacy and safety of regorafenib for advanced gastrointestinal stromal tumours after failure of imatinib and sunitinib (GRID): an international, multicentre, randomised, placebo-controlled, phase 3 trial. Lancet 2013;381:295–302.
11. Dematteo RP, Heinrich MC, El-Rifai WM, Demetri G. Clinical management of gastrointestinal stromal tumors: before and after STI-571. Hum Pathol 2002;33:466–77.
12. Balachandran VP, Cavnar MJ, Zeng S, Bamboat ZM, Ocuin LM, Obaid H, et al. Imatinib potentiates antitumor T cell responses in gastrointestinal stromal tumor through the inhibition of Ido. Nat Med 2011;17:1094–100.
13. Cavnar MJ, Zeng S, Kim TS, Sorenson EC, Ocuin LM, Balachandran VP, et al. KIT oncogene inhibition drives intratumoral macrophage M2 polarization. J Exp Med 2013;210:2873–86.
14. Medina BD, Liu M, Vitiello GA, Seifert AM, Zeng S, Bowler T, et al. Oncogenic kinase inhibition limits Batf3-dependent dendritic cell development and antitumor immunity. J Exp Med 2019;216:1359–76.
15. Seifert AM, Zeng S, Zhang JQ, Kim TS, Cohen NA, Beckman MJ, et al. PD-1/PD-L1 blockade enhances T-cell activity and antitumor efficacy of imatinib in gastrointestinal stromal tumors. Clin Cancer Res 2017;23:454–65.
16. Vitiello GA, Bowler TG, Liu M, Medina BD, Zhang JQ, Param NJ, et al. Differential immune profiles distinguish the mutational subtypes of gastrointestinal stromal tumor. J Clin Invest 2019;129:1863–77.
17. Zhang JQ, Zeng S, Vitiello GA, Seifert AM, Medina BD, Beckman MJ, et al. Macrophages and CD8(+) T cells mediate the antitumor efficacy of combined CD40 ligation and imatinib therapy in gastrointestinal stromal tumors. Cancer Immunol Res 2018;6:434–47.
18. Gasparotto D, Sbaraglia M, Rossi S, Baldazzi D, Brenca M, Mondello A, et al. Tumor genotype, location, and malignant potential shape the immunogenicity of primary untreated gastrointestinal stromal tumors. JCI Insight 2020;5:e142560.
19. Mao X, Yang X, Chen X, Yu S, Yu S, Zhang B, et al. Single-cell transcriptome analysis revealed the heterogeneity and microenvironment of gastrointestinal stromal tumors. Cancer Sci 2021;112:1262–74.
20. D'Angelo SP, Shoushtari AN, Keohan ML, Dickson MA, Gounder MM, Chi P, et al. Combined KIT and CTLA-4 blockade in patients with refractory GIST and other advanced sarcomas: a phase Ib study of Dasatinib plus Ipilimumab. Clin Cancer Res 2017;23:2972–80.
21. Singh AS, Hecht JR, Rosen L, Wainberg ZA, Wang X, Douek M, et al. A randomized phase 2 study of Nivolumab monotherapy or Nivolumab combined with Ipilimumab in patients with advanced gastrointestinal stromal tumors. Clin Cancer Res 2021;28:84-94.
22. Sommer G, Agosti V, Ehlers I, Rossi F, Corbacioglu S, Farkas J, et al. Gastrointestinal stromal tumors in a mouse model by targeted mutation of the Kit receptor tyrosine kinase. Proc Natl Acad Sci U S A 2003;100:6706–11.
23. Epardaud M, Elpek KG, Rubinstein MP, Yonekura AR, Bellemare-Pelletier A, Bronson R, et al. Interleukin-15/interleukin-15R alpha complexes promote destruction of established tumors by reviving tumor-resident CD8+ T cells. Cancer Res 2008;68:2972–83.
24. Jameson SC, Masopust D. Understanding subset diversity in T cell memory. Immunity 2018;48:214–26.
25. Robins HS, Campregher PV, Srivastava SK, Wacher A, Turtle CJ, Kahsai O, et al. Comprehensive assessment of T-cell receptor beta-chain diversity in alphabeta T cells. Blood 2009;114:4099–107.
26. Satija R, Farrell JA, Gennert D, Schier AF, Regev A. Spatial reconstruction of single-cell gene expression data. Nat Biotechnol 2015;33:495–502.
27. Hafemeister C, Satija R. Normalization and variance stabilization of single-cell RNA-seq data using regularized negative binomial regression. Genome Biol 2019;20:296.
28. Trapnell C, Cacchiarelli D, Grimsby J, Pokharel P, Li S, Morse M, et al. The dynamics and regulators of cell fate decisions are revealed by pseudotemporal ordering of single cells. Nat Biotechnol 2014;32:381–6.
29. Andreatta M, Corria-Osorio J, Muller S, Cubas R, Coukos G, Carmona SJ. Interpretation of T cell states from single-cell transcriptomics data using reference atlases. Nat Commun 2021;12:2965.
30. Goldrath AW, Luckey CJ, Park R, Benoist C, Mathis D. The molecular program induced in T cells undergoing homeostatic proliferation. Proc Natl Acad Sci U S A 2004;101:16885–90.
31. Carmona SJ, Siddiqui I, Bilous M, Held W, Gfeller D. Deciphering the transcriptomic landscape of tumor-infiltrating CD8 lymphocytes in B16 melanoma tumors with single-cell RNA-Seq. Oncoimmunology 2020;9:1737369.
32. Scott AC, Dundar F, Zumbo P, Chandran SS, Klebanoff CA, Shakiba M, et al. TOX is a critical regulator of tumour-specific T cell differentiation. Nature 2019;571:270–4.
33. Mueller SN, Germain RN. Stromal cell contributions to the homeostasis and functionality of the immune system. Nat Rev Immunol 2009;9:618–29.

34. Ebert PJR, Cheung J, Yang Y, McNamara E, Hong R, Moskalenko M, et al. MAP kinase inhibition promotes T cell and anti-tumor activity in combination with PD-L1 checkpoint blockade. Immunity 2016;44:609–21.
35. Singh MD, Ni M, Sullivan JM, Hamerman JA, Campbell DJ. B cell adaptor for PI3-kinase (BCAP) modulates CD8(+) effector and memory T cell differentiation. J Exp Med 2018;215:2429–43.
36. Geginat J, Lanzavecchia A, Sallusto F. Proliferation and differentiation potential of human CD8+ memory T-cell subsets in response to antigen or homeostatic cytokines. Blood 2003;101:4260–6.
37. Verma K, Ogonek J, Varanasi PR, Luther S, Bunting I, Thomay K, et al. Human CD8$^+$ CD57$^-$ TEMRA cells: too young to be called "old". PLoS One 2017;12: e0177405.
38. Hand TW, Cui W, Jung YW, Sefik E, Joshi NS, Chandele A, et al. Differential effects of STAT5 and PI3K/AKT signaling on effector and memory CD8 T-cell survival. Proc Natl Acad Sci U S A 2010;107:16601–6.
39. Stoklasek TA, Schluns KS, Lefrancois L. Combined IL-15/IL-15Ralpha immunotherapy maximizes IL-15 activity in vivo. J Immunol 2006;177:6072–80.
40. Margolin K, Morishima C, Velcheti V, Miller JS, Lee SM, Silk AW, et al. Phase I trial of ALT-803, a novel recombinant IL15 complex, in patients with advanced solid tumors. Clin Cancer Res 2018;24:5552–61.
41. Liu M, Etherington MS, Hanna A, Medina BD, Vitiello GA, Bowler TG, et al. Oncogenic KIT modulates type I IFN-mediated antitumor immunity in GIST. Cancer Immunol Res 2021;9:542–53.
42. Sade-Feldman M, Yizhak K, Bjorgaard SL, Ray JP, de Boer CG, Jenkins RW, et al. Defining T cell states associated with response to checkpoint immunotherapy in melanoma. Cell. 2018;175:998–1013.
43. Rusakiewicz S, Semeraro M, Sarabi M, Desbois M, Locher C, Mendez R, et al. Immune infiltrates are prognostic factors in localized gastrointestinal stromal tumors. Cancer Res 2013;73:3499–510.
44. Klaver Y, Rijnders M, Oostvogels A, Wijers R, Smid M, Grunhagen D, et al. Differential quantities of immune checkpoint-expressing CD8 T cells in soft tissue sarcoma subtypes. J Immunother Cancer 2020;8: e000271.
45. Chalmers ZR, Connelly CF, Fabrizio D, Gay L, Ali SM, Ennis R, et al. Analysis of 100,000 human cancer genomes reveals the landscape of tumor mutational burden. Genome Med 2017;9:34.
46. Offin M, Rizvi H, Tenet M, Ni A, Sanchez-Vega F, Li BT, et al. Tumor mutation burden and efficacy of EGFR-tyrosine kinase inhibitors in patients with EGFR-mutant lung cancers. Clin Cancer Res 2019;25:1063–9.
47. Jardim DL, Goodman A, de Melo Gagliato D, Kurzrock R. The challenges of tumor mutational burden as an immunotherapy biomarker. Cancer Cell 2021; 39:154–73.
48. DeMatteo RP, Lewis JJ, Leung D, Mudan SS, Woodruff JM, Brennan MF. Two hundred gastrointestinal stromal tumors: recurrence patterns and prognostic factors for survival. Ann Surg 2000;231:51–8.
49. Rosenberg SA. IL-2: the first effective immunotherapy for human cancer. J Immunol 2014;192:5451–8.
50. Kobayashi H, Carrasquillo JA, Paik CH, Waldmann TA, Tagaya Y. Differences of biodistribution, pharmacokinetics, and tumor targeting between interleukins 2 and 15. Cancer Res 2000;60:3577–83.
51. Pinette A, McMichael E, Courtney NB, Duggan M, Benner BN, Choueiry F, et al. An IL-15-based superagonist ALT-803 enhances the NK cell response to cetuximab-treated squamous cell carcinoma of the head and neck. Cancer Immunol Immunother 2019;68:1379–89.
52. Wrangle JM, Velcheti V, Patel MR, Garrett-Mayer E, Hill EG, Ravenel JG, et al. ALT-803, an IL-15 superagonist, in combination with nivolumab in patients with metastatic non–small cell lung cancer: a nonrandomised, open-label, phase 1b trial. Lancet Oncol 2018;19:694–704.